TU Delft

Delft University of Technology

Effect of peptide aerogel composite on silver nanoparticles as a catalyst for electrochemical CO_2 reduction

Rashid, Roomina; Abdinejad, Maryam; Motlagh, Mozhgan Khorasani; Noroozifar, Meissam; Kraatz, Heinz Bernhard

DOI
10.1016/j.jece.2023.110567

Publication date
2023

Document Version
Final published version

Published in
Journal of Environmental Chemical Engineering

Citation (APA)
Rashid, R., Abdinejad, M., Motlagh, M. K., Noroozifar, M., & Kraatz, H. B. (2023). Effect of peptide aerogel composite on silver nanoparticles as a catalyst for electrochemical CO_2 reduction. *Journal of Environmental Chemical Engineering*, *11*(5), Article 110567. https://doi.org/10.1016/j.jece.2023.110567

Important note
To cite this publication, please use the final published version (if applicable).
Please check the document version above.

Copyright
Other than for strictly personal use, it is not permitted to download, forward or distribute the text or part of it, without the consent of the author(s) and/or copyright holder(s), unless the work is under an open content license such as Creative Commons.

Takedown policy
Please contact us and provide details if you believe this document breaches copyrights.
We will remove access to the work immediately and investigate your claim.

This work is downloaded from Delft University of Technology.
For technical reasons the number of authors shown on this cover page is limited to a maximum of 10.

Green Open Access added to TU Delft Institutional Repository

'You share, we take care!' - Taverne project

https://www.openaccess.nl/en/you-share-we-take-care

Otherwise as indicated in the copyright section: the publisher is the copyright holder of this work and the author uses the Dutch legislation to make this work public.

Journal of Environmental Chemical Engineering 11 (2023) 110567

Contents lists available at ScienceDirect

Journal of Environmental Chemical Engineering

journal homepage: www.elsevier.com/locate/jece

Effect of peptide aerogel composite on silver nanoparticles as a catalyst for electrochemical CO_2 reduction

Roomina Rashid [a,c], Maryam Abdinejad [b], Mozhgan Khorasani Motlagh [a], Meissam Noroozifar [a,*], Heinz-Bernhard Kraatz [a,c,**]

[a] Department of Physical and Environmental Sciences, University of Toronto Scarborough, 1265 Military Trail, Toronto, ON M1C 1A4, Canada
[b] Department of Chemical Engineering, Delft University of Technology, Van der Maasweg 9, Delft 2629 HZ, the Netherlands
[c] Department of Chemistry, University of Toronto, 80 St. George Street, Toronto, ON M5S 3H6, Canada

ARTICLE INFO

Editor: Dong-Yeun Koh

Keywords:
Peptide
Silver
Aerogel
Graphene oxide
CO_2 electroreduction

ABSTRACT

Electrochemical reduction of carbon dioxide (CO_2RR) product distribution has been found to be dependent on several key factors, such as catalyst surface morphology, stability, and porosity. Metal-modified carbon-based materials have received a lot of attention in CO_2RR. However, designing a highly active metal carbon catalyst for CO_2RR utilizing low-cost chemical precursors remains a challenge. Here, a series of myristic acid-Phe-Phe peptide (MA-FF) aerogel materials containing graphene oxide (Gox) and Ag nanoparticles have been prepared for electrochemical CO_2RR. The morphologies of the composites were studied by scanning electron microscopy (SEM), and their surface compositions were determined using X-ray photoelectron spectroscopy (XPS). While the peptide aerogel alone showed no catalytic activity for CO_2 electroreduction, the addition of Ag nanoparticles results in a Faradaic efficiency (FE) of 46% for electroreduction of CO_2 to CO at an overpotential of − 0.8 V *vs.* RHE. Incorporation of Gox in the aerogel increases the FE to 88% and allows CO_2 reduction at a lower overpotential of − 0.7 V *vs.* RHE. Using highly porous peptide aerogels-Gox in addition to the metal active center provides an enhanced and new method for CO_2 conversion using low environmental impact bio-based aerogels.

1. Introduction

Human activities are the primary contributor to CO_2 emissions resulting in climate change [1,2]. An innovative strategy to mitigate the levels of atmospheric CO_2 is the capture and electroreduction of CO_2 to value-added materials [3–5]. Electrochemical CO_2 reduction reaction (CO_2RR) is a multi-proton electron transfer process which results in various reduction products [6] such as carbon monoxide (CO), formate (HCOOH), methanol (CH_3OH), ethylene (C_2H_4), ethanol (C_2H_5OH), and propanol (C_3H_7OH) [7–9]. Among these products, the CO_2RR of CO_2 to CO is a profitable alternative to traditional methods of CO procurement and is driven by demand for CO as a starting material for the widespread synthetic workflows, such as the Fischer-Tropsch process [10,11]. CO_2RR currently faces limitations due to a need for electrocatalysts that allow for efficient adsorption, activation, and desorption of the highly inert and stable CO_2 molecule [7]. Designing an electrocatalytic system with high current density, stability, and selectivity at low overpotentials is necessary to bring this technology closer to industrial implementation [8].

Among several transition metal catalysts, metallic silver (Ag) is well known as an effective electrocatalyst for converting CO_2 to CO selectively. By itself, metallic Ag requires high overpotentials to reduce CO_2 and suffers from competitive competition with side reactions such as hydrogen evolution reactions (HERs); however, advances that favourably modulate the morphology of Ag-based materials have addressed some of these challenges.

Nanostructured Ag-based catalysts with the increased surface area have been developed to improve the CO_2 reduction activity of metallic Ag [12,13]. Qi Lu et al. reported a nanoporous Ag catalyst for electroreduction of CO_2 to carbon monoxide with approximately 92% selectivity over 3000 times higher than polycrystalline Ag under moderate overpotentials of 0.50 V [14]. Additionally, others have shown that a Ag nano-coral catalyst can exhibit a 32-fold increase in surface-area-normalized activity compared to Ag foil at an overpotential

* Corresponding author.
** Corresponding author at: Department of Physical and Environmental Sciences, University of Toronto Scarborough, 1265 Military Trail, Toronto, ON M1C 1A4, Canada.
E-mail addresses: m.noroozifar@utoronto.ca (M. Noroozifar), bernie.kraatz@utoronto.ca (H.-B. Kraatz).

https://doi.org/10.1016/j.jece.2023.110567
Received 20 February 2023; Received in revised form 15 June 2023; Accepted 14 July 2023
Available online 17 July 2023
2213-3437/Crown Copyright © 2023 Published by Elsevier Ltd. All rights reserved.

of 0.49 V [15].

Carbon-supported catalysts have been made using a variety of carbon materials such as graphite, carbon black, carbon fibres, glassy carbon, pyrolytic carbon, polymer-derived carbon, graphene oxide, fullerenes, and carbon nanotubes (CNTs) [16]. Carbon supports are cost-effective with unique properties including tunablity [17], high surface area [18], and high electrical conductivity [19,20] that can enhance the overall electrocatalyst activity towards CO_2RR. Modification of Ag-based catalysts using carbon supports can improve electrocatalyst performance [21,22]. Kim et al. have reported Ag nanoparticles immobilized on carbon supports [21]. Modification of Ag with conductive carbon support has helped to reduce the overpotential needed for Ag-mediated CO_2RR as well as result in a 4-fold increase in CO production; with a high current density of 350 mA cm^{-2} as well as a high Faradaic efficiency (FE) of $>$ 95% for CO [23].

Aerogels have been shown in studies to help increase catalytic surface area by expanding the catalytic active surface area to maximize mass transport [24–26]. Aerogels have three-dimensional supramolecular porous structures with large and tunable surface areas, high stability, thermal conductivity, intricate microstructures, low density and hydrophobicity [27,28]. Their porous structure increases the access of electrons to the catalyst, significantly increasing its charge transfer capacity [29]. Abdinejad et al. have reported a Ag-Pd bimetallic aerogel with CNTs to convert CO_2 to CO with a FE of 91% at a low overpotential of − 0.7 V *vs.* RHE [30].

Bio-based aerogels made from materials such as lignin, pectin, cellulose, and proteins possess excellent porous structures, high stabilities, and a lower environmental impact due to being biodegradable and non-toxic when compared to inorganic aerogels [31,32]. For example, AgCu nanoparticle/ Silk fibroin-derived carbon aerogel showed a good FE_{CO} of 71% at 1.26 V *vs.* RHE, and a significant current density of 15.77 mA cm^2 towards CO at 1.06 V *vs.* RHE [33]. Although these materials have gained significant attention in recent years for CO_2 capture and reduction; inadequate literature is present for these materials [32].

In order to advance the field of bio-based CO_2RR catalysts, we have developed a bio-based catalyst with high selectivity and high current density for CO_2 reduction as part of our ongoing study using various bimetallic aerogel materials with carbonaceous support for CO_2 electroreduction. Previously, our group has worked on the development of a peptide conjugate hydrogel; myristic acid-phe-phe-OH (MA-FF) [34]. MA-FF is reported to have a high-stability nanofiber matrix which consists of β-sheet aggregates and exposed functional groups providing a tunable surface area [34]. Herein, we report an aerogel-based composite consisting of MA-FF, graphene oxide (Gox), and Ag that acts as a catalyst for CO_2 electroreduction. A series of these composites were prepared with varying ratios of Gox to Ag for systematic comparison. The composite with a Gox:Ag ratio of 2:1 exhibited the greatest ability to reduce CO_2 to CO with a FE_{CO} of 88% at a low overpotential of − 0.7 V *vs.* RHE. This work introduces peptide materials as a new class of readily accessible scaffolds that can serve in electrocatalysis reactions.

2. Materials and methods

2.1. Reagents and chemicals

All chemicals and reagents were used as received, with no further purification unless noted. Methyl esters of amino acids were purchased from Advanced Chem.Tech. and Sigma-Aldrich. Myristic acid, graphite flakes (<20 μm), H_2SO_4, $NaNO_3$, $KMnO_4$, $NaBH_4$, $AgNO_3$, NaH_2PO_4, $NaHCO_3$, and Nafion per fluorinated ion-exchange resin (5%) were purchased from Sigma-Aldrich. Deionized water from a Millipore MilliQ water purification system (18.2 MΩ cm) was used to prepare all experimental solutions. Myristic acid-phe-phe-OH (MA-FF) peptide conjugate was synthesized as previously reported by Falcone et al. [35].

2.2. Graphene exfoliation

Delamination of graphene was done using a modified version of the well-known Hummers method.[36] $NaNO_3$ was combined with graphite powder in a 1:1 ratio. Next, H_2SO_4 was added to the solution while keeping in an ice bath with constant stirring for 2 h. $KMnO_4$ was added to the solution while keeping a contained temperature below 15 °C. The solution was left to stir at room temperature for 2 days until a pasty brown solution was achieved. A 1:1 solution of H_2O_2 and de-ionized water was added to the pasty brown solution and left in fridge for 2 days. Yellow solution was decanted off and the brown slurry was washed twice with 10% HCl. Liquid on top was disposed of and solid graphene oxide (Gox) at bottom was washed twice with de-ionized H_2O and placed in an oven at 75 °C for 24 h to dry.

2.3. Silver particles

A solution of 1:1 $AgNO_3$ and $NaBH_4$ was prepared by adding 1 mL of 2 M $NaBH_4$ solution drop wise to 1 mL of 2 M $AgNO_3$ solution. The reaction flask was kept on ice during this time. The solution effervesced and changed color from yellow to grey/black clumps in solution. The solution was left to sit overnight and solid was washed three times with de-ionized water the next day. Reduced Ag particles were collected and dried in an oven for 24 h at 50 °C.

2.4. Aerogels of MA-FF

5 mg of the MA-FF powder was added to a vial along with 1 mL NaH_2PO_4 solution (pH 7.1). The gel was prepared of 0.5% as reported before [35]. The vial was heated in an oil bath at 85 °C. The heat aids in the dissolution of the gelator in an aqueous solution. The vial was left undisturbed to cool down during which the hydrogel formed via self-assembly of the peptide fibers. The gel remained intact which was indication of a solid gel material. The hydrogel was lyophilized and freeze-dried to maintain the porous structure while removing all liquid.

2.5. Aerogels of mixture of MA-FF and Gox (MA-FF+Gox)

0.5 mL NaH_2PO_4 solution (pH 7.1) was added to 5 mg peptide conjugate and dissolved using an oil bath at 85 °C. 0.5 mL of 0.5% Gox solution (5 mg Gox in 1 mL NaH_2PO_4 solution with pH 7.1) was immediately transferred to the gel vial and mixed thoroughly. The gel was then allowed to cool down on the bench during which the self-assembly and hydrogel formation occurred. The hydrogel was lyophilized and freeze-dried.

2.6. Aerogels of mixture of MA-FF and Ag (MA-FF+Ag)

0.5 mL of NaH_2PO_4 solution (pH 7.1) was added to 5 mg peptide conjugate and dissolved by heating in an oil bath at 85 °C. 0.5 mL of 0.5% Ag solution (5 mg Ag in 1 mL NaH_2PO_4 solution with pH 7.1) was immediately transferred to the gel vial and mixed thoroughly. The gel was then allowed to cool down on the bench during which the self-assembly and hydrogel formation occurred. The hydrogel was lyophilized and freeze-dried.

2.7. Aerogels of mixture of MA-FF, Gox, and Ag with different ratios of Gox and Ag: MA-FF+ Gox+ Ag (1:1), MA-FF+ Gox+ Ag (1:2) and MA-FF+ Gox+ Ag (2:1)

For example, for the preparation of aerogel of mixture of MA-FF, Gox, Ag in 1:1 ratio of Gox:Ag (MA-FF+ Gox+ Ag (1:1)), 0.5 mL of NaH_2PO_4 solution (pH 7.1) was added to 5 mg peptide conjugate, the solution was sonicated for 5 min and the contents were further dissolved using an oil bath at approximately 75–80 °C. 0.5 mL of a solution containing 5 mg Gox and 5 mg Ag in 1 mL NaH_2PO_4 solution was

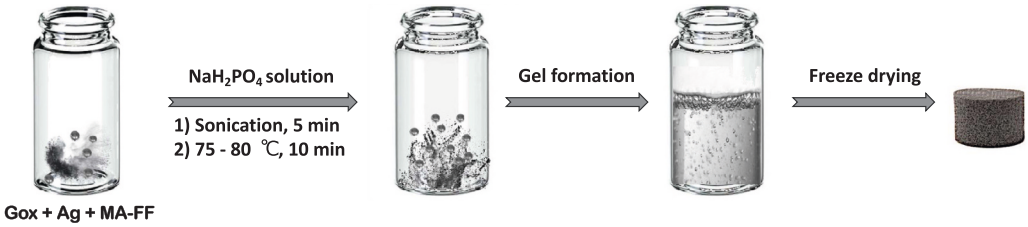

Scheme 1. Schematic of aerogel composites preparation.

immediately transferred to the gel vial and mixed thoroughly. The gel was then allowed to cool down undisturbed, during which the self-assembly took place and hydrogel formation occurred. The hydrogel was lyophilized and freeze-dried. In the same manner, aerogels MA-FF+ Gox+ Ag (1:2), MA-FF+ Gox+ Ag (2:1) were synthesized as shown in SI and Scheme 1.

2.8. Apparatus

Field-Emission Scanning Electron Microscope (FISEM) and elemental mapping analyses for the samples was done using the Hitachi 5700 Scanning Electron Microscope (SEM, Hitachi, Chiyoda, Tokyo, Japan) and a Quanta Feg 250 Field-Emission Scanning Electron Microscope. X-ray photoelectron spectroscopy (XPS) measurements were obtained using the Thermo Fisher Scientific K-Alpha XPS spectrometer (Thermo Fisher Scientific - E. Grinstead, UK) located at the Ontario Centre for the Characterization of Advance Materials (OCCAM). Survey spectra (nominal 400 μm spot, 200 eV pass energy (PE), 1 eV step size) were obtained for all samples followed by low-resolution spectra (150 eV pass energy, 0.2 eV step size) on the spectral regions of interest (Ag 3d, C 1 s, N 1 s, O 1 s) from which the composition was obtained. Spectra processing was done using the system's software (Avantage v5.986) and for the baseline a modified Shirley background was used.

2.9. Characterization of CO_2 electroreduction products

The gaseous products (CO_2, H_2) were analyzed using a gas chromatography (GC, InterScience PerkinElmer Clarus 680) coupled with two thermal conductivity detectors (TCD) and a flame ionization detector (FID). An average of four injections was used to determine the concentration of gaseous products in gas chromatography. This was then used to calculate their Faradaic efficiencies. The liquid product was analyzed using HPLC (Infinity 1260 II LC, Agilent Technologies. Hi-Plex H column (50 °C) with VWD (210 and 280 nm) and RID (40 °C). ^{1}H NMR was done using Bruker 400 MHz and was processed in MestreNova.

2.10. Electrochemical measurements

For the electrochemical reactions, the $NaHCO_3$ buffer solutions with pH 7.5 were saturated with Ar or CO_2 and the remaining experiment was

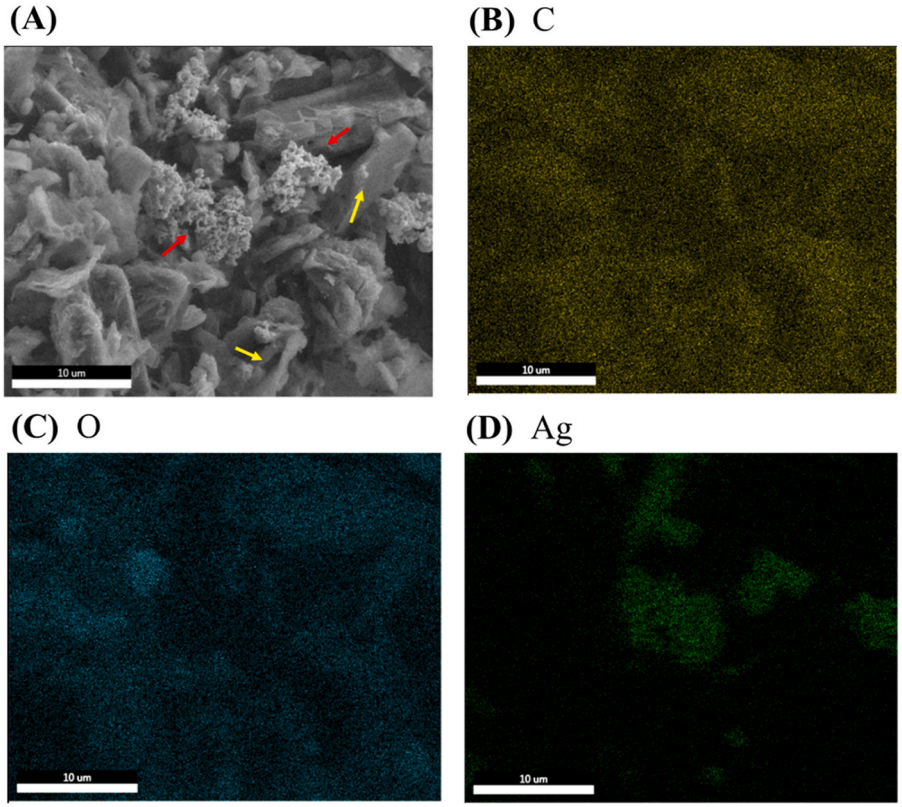

Fig. 1. (A) Scanning Electron Microscopy (SEM) image of MA-FF + Gox + Ag (2:1) aerogel with a scale bar of 10 μm, (B-D) elemental mapping of C, O, and Ag respectively with a scale bar of 10 μm.

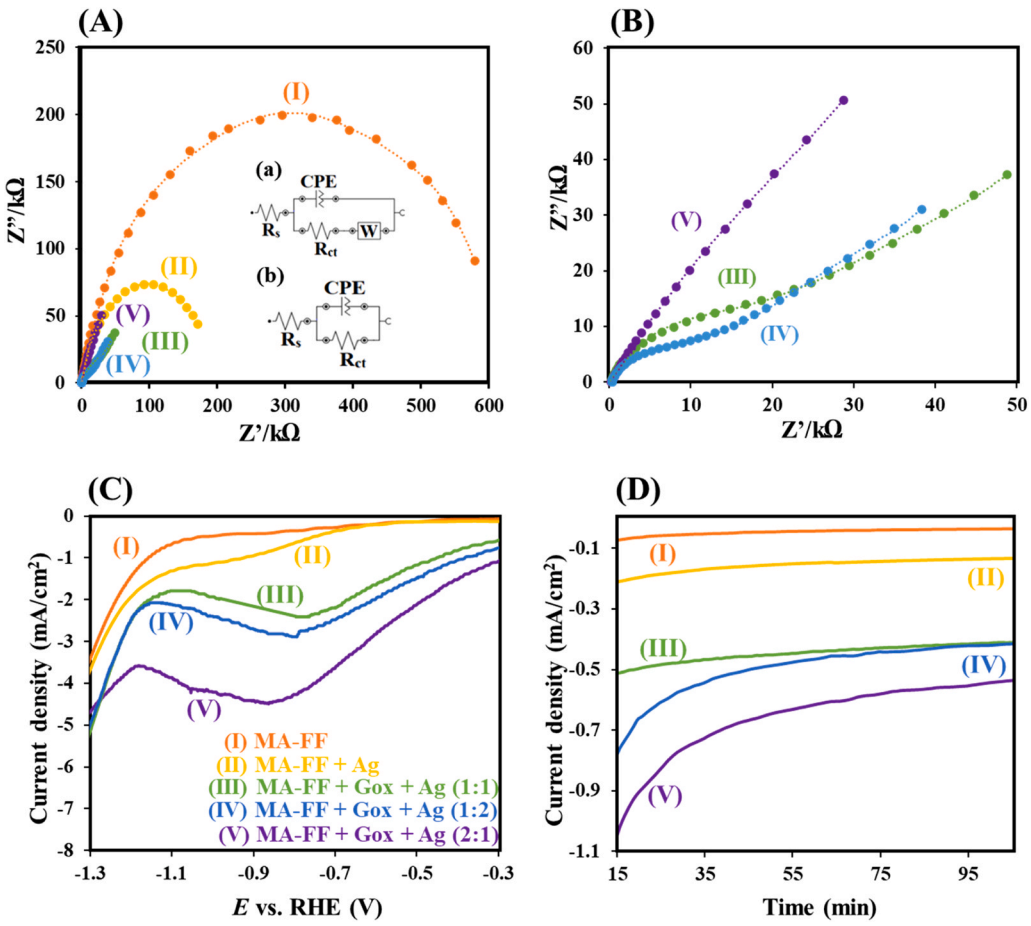

Fig. 2. (A) Nyquist plots and fitting data of MA-FF co-gels at an amplitude of 5 mV with a frequency range from 10 kHz to 0.01 Hz, (a) and (b) are two different fitted equivalent circuits, (B) Nyquist plots for Nyquist plots MA-FF + Gox + Ag (1:1), MA-FF + Gox + Ag (1:2) and MA-FF + Gox + Ag (2:1) with different magnification, (C) Linear sweep voltammetry (LSV) comparison of MA-FF co-gels, (D) chronoamperometry (CA) comparison of MA-FF co-gels at − 0.7 V *vs.* RHE, in 0.1 M $NaHCO_3$ saturated with CO_2.

performed in sealed conditions. A CHI 660 C potentiostat (CH Instruments, Austin, TX) with a three-electrode setup enclosed in a Faraday cage was used for the electrochemical studies. The three electrodes used were 1) modified glassy carbon electrode (GCE) with different aerogel modifiers (i.d. = 3 mm) as working electrode, 2) Pt wire as auxiliary electrode and 3) Ag/AgCl as reference electrode.

Prior to deposition on the GCEs, the electrodes were polished using 1, 0.3, and 0.05 μm alumina in sequence for 15 min, each. The GCEs were cleaned further by ultrasonication in water and ethanol for 10 min, each. 2 mg of aerogel modifier was dispersed in 50 μL Nafion solution 2%. The solution was vortexed for 5 min to thoroughly mix it before being homogenized in an ultrasonic bath for 10 min 3 μL of this solution was drop casted on the surface of GCE and left to dry overnight.

A H-cell with 50 mL was used for CO_2 electroreduction study. The anodic and cathodic chambers of the H-cell containing 0.1 M $NaHCO_3$ buffer solution with pH 7.5 and are separated by a Nafion-117 membrane. Linear sweep voltammetry (LSV) measurements were conducted with a positive initial scan polarity, 5- second quiet, and a scan rate of 0.1 V/s. All potentials were converted from Ag/AgCl (3 M KCl) to RHE ($E_{RHE}=E^0_{Ag/AgCl} + 0.0591 \times pH + 0.210$). The reported Faradaic efficiency (FE) and current density (j) are average values based on five reactions run with GC measurements taken every 15 min for 2.5 h. It should be noted that all the reported current density has been calculated based on the geometrical electrode dimensions (3 mm diameter).

The faradic efficiency (%) of the gaseous products (here denoted as " i ") were quantified according to the formula;

$$FE(i)\% = \frac{n_i \bullet F \bullet \phi_i \bullet \upsilon_{MFM}}{I} \quad (1)$$

where "n_i" is the number of the electrons needed for CO_2 reduction to product " i ", "F "is the Faraday constant, "ϕ_i" is the volume fraction of the gases, " I " is the current measured at the time of the injection, and "υ_{MFM}" is the molar gas flow rate measured by mass flow meter at the cell outlet and corrected according to the product mixture. The gas outlet of the H-cell electrolysis was connected to the sampling port of the GC, which injects a certain volume of the pre-chamber filled with saturated product gas from CO_2 electrolysis. An injection loop takes around 5 min including the back-flush and stabilization time. A Molsieve-S4 column connected to a thermal conductivity detector (TCD) was used to analyze hydrogen (H_2) and carbon monoxide (CO) gases.

3. Results and discussion

3.1. Characterization of the peptide aerogels

Scanning electron microscopy (SEM) was used to examine the morphological characteristics of the MA-FF, MA-FF + Gox, MA-FF + Ag, MA-FF+ Gox+ Ag (1:1), MA-FF+ Gox+ Ag (1:2), MA-FF+ Gox+ Ag (2:1) aerogels (Fig. 1 and Fig. S1). The porous, sponge-like nature of the aerogel is a common feature of the prepared various aerogels. The intertwined fibrous network has been reported to be an indication of strong peptide gel materials [34–36]. When Gox is added, the peptide

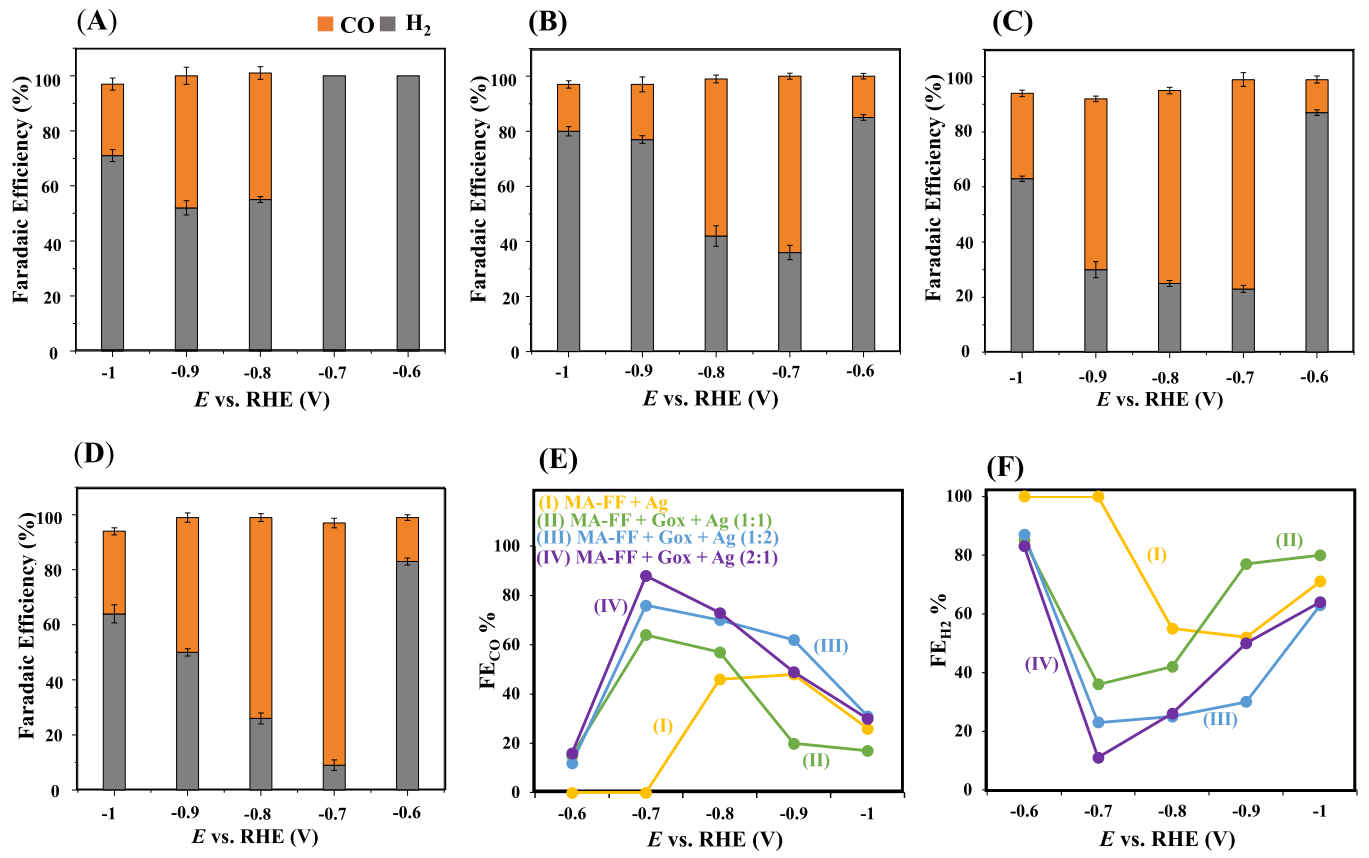

Fig. 3. CO and H_2 Faradaic efficiencies comparison of (A) MA-FF + Ag, (B) MA-FF + Gox + Ag (1:1), (C) MA-FF + Gox + Ag (1:2) and (D) MA-FF + Gox + Ag (2:1) at different potentials of − 0.6 V, − 0.7 V, − 0.8 V, − 0.9 V and − 1.0 V *vs.* RHE in 0.1 M $NaHCO_3$. Comparing (E) FE_{CO} and (F) FE_{H2} of MA-FF co-gels at different potentials of − 0.6 V, − 0.7 V, − 0.8 V, − 0.9 V and − 1.0 V *vs.* RHE in 0.1 M $NaHCO_3$.

matrix changes, revealing opaque sheet-like structures within the peptide gel. The presence of Gox appears to have no effect on the peptide fibrous network. Gox forms non-covalent bonds, mainly π–π stacking bond interactions between Gox sheets and the peptides' phenyl groups, which improves gel formation and strength [37]. The overall architecture appears more intricate, indicating a potential increase in surface area, which could aid in CO_2 capture (Fig. S1a). When Ag is added, it appears in small clusters entrapped across the peptide gel matrix. These metal clusters interfere with the peptide conjugate's self-assembling fibrous structure (Fig. S1c). On the other hand, the addition of both Gox and Ag nanoparticles to the MA-FF gel, improves the overall structure of the aerogel. The porosity and fibrous nature of the aerogel matrix increases as Ag nanoparticles are entrapped across the matrix. The overall structure is heavily influenced by the ratio of Gox:Ag nanoparticles present in the sample. As demonstrated here, a higher Gox content promotes better structure formation with the MA-FF conjugate, allowing for better entrapment of Ag nanoparticles within the aerogel (Fig. S1d-f).

The presence of Gox sheets within the aerogel (yellow arrows in Fig. 1A) indicates the presence of sheet-like structure within the aerogel, which enhances the three-dimensional architecture of the peptide gel. The Ag particles entrapped within the MA-FF and Gox aerogel for CO_2 capture and reduction are represented by the small particulate matter (red arrows in Fig. 1A). The elemental mapping of the MA-FF-Gox-Ag (2:1) is depicted in Fig. 1B-D. The presence of carbon, oxygen, and Ag elements within the multi-component aerogel is confirmed by their distribution throughout the aerogel matrix which can lead to increase in the CO_2RR activity. SEM with the backscattered electron detector (SEM-BSD) in Figs. S2-S4 were acquired to confirm the presence of Ag nanoparticles and visually observe the varying contents of Ag in the different ratio aerogels. The amount of Ag present in the aerogels can be correlated with the bright spots in these images [38], and the dispersion of the Ag nanoparticles in the aerogels is clearly demonstrated in these Figures.

The surface composition of the MA-FF, MA-FF + Gox, and MA-FF + Gox + Ag aerogels was determined using X-ray photoelectron spectroscopy (XPS) (Figs. S5-S9). The characteristic peaks such as C 1 s, O 1 s, and N 1 s were revealed by XPS analysis. In the survey, two distinct peaks were observed at binding energies of 368.1, and 374.1 eV in the MA-FF + Gox + Ag aerogel, which were absent in the MA-FF and MA-FF + Gox aerogels, and these two peaks are attributed to Ag $3d_{3/2}$ and Ag $3d_{5/2}$, respectively. These binding energies are slightly lower than the individual Ag binding energies of 368.6 for Ag $3d_{3/2}$ and 374.6 eV for Ag $3d_{5/2}$, indicating partial electron transfer between the Ag and composite. These findings confirmed the presence of metallic silver, which is the active site for CO_2 reduction in the prepared aerogel. A peak for O 1 s is present at 531.48 eV for MA-FF aerogel, and the value is shifted to a slightly higher binding energy of 531.68 eV for MA-FF + Gox and 531.88 for MA-FF + Gox + Ag. When materials are added to the peptide gel, the electron chemical environment changes, causing the binding energy to shift. The increased charge transfer and insulation effect of the Gox sheets contribute to a synergistic effect between the additives and the peptide, resulting in a shift in the binding energy in the Gox-containing peptide aerogels [38]. The N 1 s peak at 399.4 eV is contributed by the amide bond of the peptide conjugate, and the C 1 s peak at 284.5 eV is contributed by the peptide as well as Gox [37].

Electrochemical impedance spectroscopy (EIS) study was used to

measure the attribution of conductivity (or nature of the charge-transfer resistance) of the MA-FF, MA-FF + Ag, MA-FF + Gox + Ag(1:1), MA-FF + Gox + Ag(1:2) and MA-FF + Gox + Ag (2:1). The Nyquist plots, fitting results, and the corresponding equivalent Randles' circuit are shown in Fig. 2 A and B. In the equivalent Randles' circuit, R_s, C_{dl}, R_{ct}, Z_w, and CPE are the uncompensated solution resistance, double-layer capacitance, charge transfer, mass-transport contribution (Warburg resistance) for ion diffusion, and the constant phase element (which accounts for the bulk capacitance of the catalyst), respectively. The results for equivalent Randle's circuit of the catalysts were summarized in Table S1. The MA-FF and MA-FF + Ag were fitted with equivalent circuit "a" whereas MA-FF + Gox + Ag (1:1), MA-FF + Gox + Ag (1:2) and MA-FF + Gox + Ag (2:1) were fitted with equivalent circuit "b". Equivalent circuit of MA-FF and MA-FF + Ag contained R_s, CPE, and R_{ct} without Z_w because the semi-circle did not exhibit any noticeable diffusive element. According to Table S1, MA-FF has a R_{ct} of 590 KΩ which means there is a very high resistance to flow of current within this sample, however when Ag is incorporated the R_{ct} drops to 163.9 KΩ. For both these samples, there was limited charge transfer and consequently no diffusion was observed and no Zw was reported. It is possible that R_{ct} decline is because the MA-FF and Ag reduce overall coverage on the electrode surface giving way to some charge transfer. Addition of Gox to the peptide-Ag samples significantly reduced the Rct and exhibited ion diffusion. An Rct of 19.4, 10.1 and 0.136 KΩ is reported for MA-FF + Gox + Ag (1:1), MA-FF + Gox + Ag (1:2) and MA-FF + Gox + Ag (2:1) respectively. This decline in R_{ct} indicates reduction in the resistance of the sample and consequently increase in the ability to relay a charge in the samples. This supports the idea that Gox inclusion helps induce flow of charges within the samples which helps produce materials suitable for CO2RR. Warburg resistance was reported as 24.7, 29.0 and 11.3 $\mu Mho \times S^{1/2}$ for MA-FF+ Gox+ Ag (1:1), MA-FF+ Gox+ Ag (1:2) and MA-FF+ Gox+ Ag (2:1) respectively. The slight decrease in the Zw of (1:2) aerogel to the (2:1) aerogel could be attributed to increased spaces between the Gox sheets in the (2:1) ratio which reduces the ionic diffusion slightly.

3.2. *Electroreduction of CO_2 by the peptide aerogels*

Using linear sweep voltammetry (LSV), the electrocatalytic capabilities of the peptide aerogels were investigated, and the results are shown in Fig. 2 C. A compartment electrochemical H-Cell system was used as an electrochemical cell containing a Nafion membrane with a three-electrode system including Ag/AgCl reference electrode, a glassy carbon electrode (GCE) modified with the synthesized peptide aerogels and a platinum auxiliary electrode. The electrocatalytic activity of the modified GCE electrodes toward CO_2RR was measured in 0.1 M $NaHCO_3$ electrolyte saturated with Ar and later with CO_2. The current density of modified GCE with peptide aerogel was increased after exposure to CO_2. MA-FF + Gox + Ag (2:1) showed the highest current density at - 0.8 V *vs.* RHE, followed by MA-FF + Gox + Ag (1:2), MA-FF + Gox + Ag (1:1), MA-FF + Ag, and then MA-FF in decreasing current density order. MA-FF aerogel alone has the lowest current density, demonstrating how the addition of Gox and Ag within these peptide aerogels can improve CO_2 capture and reduction.

The catalytic activity and selectivity of the aerogels was examined using the chronoamperometry technique at several potentials of − 0.6, − 0.7, − 0.8, − 0.9, and 1.0 V *vs.* RHE in 0.1 M $NaHCO_3$ saturated with CO_2 to detect the optimal potential. The best selectivity was observed at − 0.7 V vs. RHE belonging to MA-FF + Gox + Ag (1:1) in 0.1 M $NaHCO_3$. Comparing the catalytic activity of all synthesized catalysts at − 0.7 V *vs.* RHE, as shown in Fig. 2D, the highest current density belongs to MA-FF + Gox + Ag (2:1), which highlights the important role of Ag in the overall catalytic activity towards CO_2.

Table 1
Summary of composition and performance metrics of H-type electrolytic cells for electrochemical conversion of CO_2 into CO using silver-based catalysts.

Cell composition	E/ V *vs.* RHE	Electrolyte concentration/ M	pH	FE (%)	Ref.
GCE/ Sponge-Like Porous Silver Nanocubes | $KHCO_3$|Nafion117| $KHCO_3$|Pt	-0.9	0.1	6.8	90	[42]
GCE/ $Ag_{88}Cu_{12}$ /GCE | $NaHCO_3$|Nafion117| $NaHCO_3$|Pt	-0.89	0.1	6.8	89.4	[43]
Carbon fiber papers- H_2-annealed Ag | $KHCO_3$|Nafion117| $KHCO_3$|Pt	-1.0	0.1	-	30	[44]
Carbon fiber papers- air-annealed Ag | KHCO3|Nafion117| KHCO3|Pt	-1.0	0.1	-	90	[44]
GCE/carbon paper disc-Ag | KHCO3|Nafion117| KHCO3|Pt	-1.2	0.5	7.0	23.5	[45]
GCE/ $Pd_{0.67}Ag_{0.33}$ aerogel| $KHCO_3$|Nafion117| $NaKCO_3$| Pt	-0.8	0.1	7.4	84	[30]
GCE/ $Pd_{0.67}Ag_{0.33}$ aerogel/ CNT| $KHCO_3$|Nafion117| $NaKCO_3$| Pt	-0.7	0.1	7.4	91	[30]
Silver hollow fiber| $KHCO_3$|Nafion117| $NaKCO_3$| Pt	-1.2	0.5	7.2	92	[46]
GCE/MA-FF-Ag /GCE | $NaHCO_3$|Nafion117| $NaHCO_3$|Pt	-0.8	0.1	7.5	46	This work
MA-FF-Gox-Ag (1:1)/GCE | $NaHCO_3$|Nafion117| $NaHCO_3$| Pt	-0.7	0.1	7.5	64	This work
MA-FF-Gox-Ag (1:2)/GCE | $NaHCO_3$|Nafion117|0.1 M $NaHCO_3$| Pt	-0.7	0.1	7.5	76	This work
MA-FF-Gox-Ag (2:1)/GCE | $NaHCO_3$|Nafion117| $NaHCO_3$| Pt	-0.7	0.1	7.5	88	This work

The gas and liquid products of the controlled potential electrolysis at the potential of − 0.6 to − 1.0 V *vs.* RHE in Fig. 3A-D and Table S2 were measured using gas chromatography (GC) and HPLC, respectively. CO and H_2 were detected as CO_2 reduction products at all potentials for all peptide aerogels, and no liquid products were detected. For example, Fig. 3D shows the results for MA-FF + Gox + Ag (2:1) with the optimal overpotential of − 0.7 V *vs.* RHE. MA-FF + Gox + Ag (2:1) had the highest selectivity towards CO_2 reduction (FE_{CO}: 88%) compared to MA-FF + Gox + Ag (1:2) (FE_{CO}: 76%) and MA-FF + Gox + Ag (1:1) (FE_{CO}: 64%) at − 0.7 V *vs.* RHE in 0.1 M $NaHCO_3$. MA-FF + Ag had a lower product selectivity (FE_{CO}: 46%) at a more negative overpotential of − 0.8 V *vs.* RHE.

Fig. 3E and F compare the CO and H_2 Faradaic efficiencies of MA-FF co-gels, and MA-FF + Gox + Ag (2:1) showed the lowest selectivity towards H_2 reduction. With an increase in negative overpotentials, there was a decrease in CO production and an increase in H_2 production due to hydrogen evolution reactions (HERs) occurring at the electrode surface in all peptide aerogels studied. These results show that doubling the amount of Gox in the Ag active centre allows for increased current density and product selectivity of the aerogel at a more positive overpotential of − 0.7 V *vs.* RHE. When compared to Gox-free aerogel, the CO_2 reduction capacity of the 2:1 aerogel significantly increases. Generally, large overpotentials contribute to damage to the catalyst and

HERs. The need for large overpotential also raises operation costs as there is now a high energy demand. This is not feasible if the catalyst is to be scaled to large scale CO_2RR [39]. The ability of this catalyst to function at less negative overpotential is beneficial as this means that there will be lesser energy consumption for this catalyst to function. Gox sheets have a larger surface area to volume ratio for CO_2 capture and reduction, whereas Ag is the active centre for CO_2RR. Gox can form non-covalent interactions such as π–π stacking with the phenyl rings of the peptide aerogel structure as well as hydrogen bonding between the exposed Gox functional groups and peptide side groups which can potentially enhance the overall surface area, induce conductivity, and provide that increased current density that we observe in the results [40]. Ag has faced the problem of aggregating and ducking in their active sites for CO_2RR when incorporated in catalysts. Possibly presence of an intricate porous structure allows the Ag to disperse across the catalyst, preventing the metal aggregation. This ensures that maximum catalytic sites are available for CO_2RR [41]. The results obtained demonstrate that the peptide aerogel's exceptional porous nature, in combination with Gox and Ag in a 2:1 ratio, provides a synergistic effect that facilitates the aerogel with enhanced catalytic activity.

These results show how simple variations in the catalyst structure as well as the applied potential can help control the type and amount of product produced. This helps create highly tunable electrocatalyst systems which can be optimized as per the need.

Table 1 provides detail for other silver-based catalysts for CO_2RR. Fan et al. reported sponge like porous Ag nanocubes on carbon paper [42]. They reported a high FE_{CO} of 93% at − 0.9 V *vs.* RHE. *Wang* et al. reported an Ag-Cu bimetallic aerogel which exhibits a FE_{CO} of 89.4% at − 0.89 V *vs*. RHE [43]. Air-annealed Ag alone and Air-annealed Ag with post-treatment H_2 thermal annealing was used for CO_2RR by Jiang et al. [44]. They reported 30% and 90% FECO at −1.0 V vs. RHE for these catalysts, respectively indicating that subsurface chemically bonded O species in Air-annealed Ag contributed to increased CO selectivity rather than H_2 in CO_2RR electrolysis. Mattarozzi et al. reported a ligand-free silver nanoparticle for CO_2RR with 23.5% FE_{CO} at −1.2 V vs. RHE [45]. Also, silver hollow fiber electrode was used for efficient CO_2RR [46] with a FE_{CO} 92% at − 1.2 V *vs.* RHE. Indeed, our group reported a Ag-Pd aerogel and Ag-Pd aerogel /CNT for CO_2RR with FE_{CO} 84% and 91% at potentials − 0.8 and − 0.7 V *vs.* RHE, respectively. These catalysts possess the same main characteristics as our composites such as high porosity, high conductivity and Ag metal as active centre for CO_2RR. The four different catalyse reported here showed FE_{CO} 46%, 64%, 76%, and 88% for MA-FF-Ag, MA-FF-Gox-Ag (1:1), MA-FF-Gox-Ag (1:2), and MA-FF-Gox-Ag (2:1) at potential − 0.7 V vs. RHE. While this may seem more attractive than the work reported here, it is important to mention that their optimal CO_2RR took place at a much higher overpotential of − 0.9 to − 1.2 V vs. RHE compared to the more positive overpotential of − 0.7 V vs. The overpotential is higher than the overpotential at which our optimized catalyst is able to produce a similarly high FE_{CO} of 88%. Finally, the liquid phase was tested using both HPLC and NMR techniques, but we have no evidence for reduction products in the liquid phase.

Silver and silver-based catalysts have shown to be high selective in the electrochemical reduction of CO_2 to CO, generally with good faradaic efficiencies and the mechanism of this transformation has been extensively studied [47–51]. In this work, there is no any products in liquid phase and only CO and H_2 detected by GC form gas phase and one may speculate that the mechanism operational in this current study is fairly analogous.

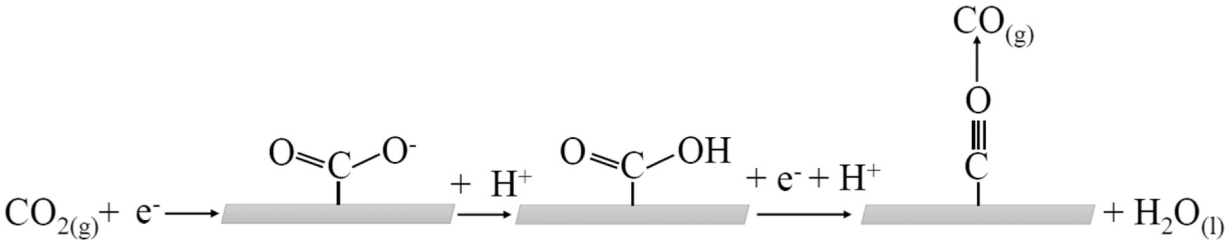

.

This suggests that CO_2 is bound to the active sites of the silver catalyst, followed by electron transfer and generation of a putative $*CO_2^{\bullet-}$ intermediate. Protonation can produce two possible intermediates *COOH or *OCHO [52–55]. In the second reduction step, CO_g and H_2O_l are released [56].

4. Conclusion

In summary, we developed a novel peptide aerogel composite acting as a catalyst, containing Gox and Ag nanoparticles for CO_2RR. The composite with Gox to Ag ratio of 2:1, provides high selectivity (FE_{CO}: 88%) and high current density at a low overpotential of − 0.7 V *vs.* RHE. When compared to non-Gox inclusion catalysts, the Gox within the catalyst structure facilitates the enhancement of catalyst architecture and increased mass and charge transfer, resulting in an increase in catalyst activity. To the best of our knowledge, this is the first report of a peptide aerogel for CO_2RR. This study opens possibilities for future research involving bio-based materials for CO_2 electroreduction, as these materials have a lower environmental impact and could potentially provide eco-friendly CO_2RR catalysts.

CRediT authorship contribution statement

Roomina Rashid: Conceptualization, Methodology, Validation, Formal analysis, Investigation, Resources, Data curation, Writing – original draft, Writing – review & editing. **Maryam Abdinejad:** Conceptualization, Methodology, Formal analysis, Investigation, Resources, Data curation, Writing – original draft, Writing – review & editing. **Mozhgan Khorasani Motlagh**: Conceptualization, Methodology, Formal analysis, Resources, Investigation, Resources, Data curation, Writing – original draft, Writing – review & editing. **Meissam Noroozifar:** Conceptualization, Methodology, Validation, Formal analysis, Investigation, Resources, Data curation, Project administration, Supervision, Writing – original draft, Writing – review & editing. **Heinz-Bernhard Kraatz**: Conceptualization, Methodology, Validation, Formal analysis, Investigation, Resources, Funding acquisition, Project administration, Supervision, Writing – review & editing. All authors have read and agreed to the published version of the manuscript.

Declaration of Competing Interest

The authors declare that they have no known competing financial interests or personal relationships that could have appeared to influence the work reported in this paper.

Data Availability

No data was used for the research described in the article.

Acknowledgments

This work was supported by Natural Sciences and Engineering Research Council of Canada (RGPIN-2022–03129), and the University of Toronto.

Appendix A. Supporting information

Supplementary data associated with this article can be found in the online version at doi:10.1016/j.jece.2023.110567.

References

[1] R. Sharifian, R.M. Wagterveld, I.A. Digdaya, C. Xiang, D.A. Vermaas, Electrochemical carbon dioxide capture to close the carbon Cycle, Energy Environ. Sci. 14 (2) (2021) 781–814, https://doi.org/10.1039/D0EE03382K.
[2] C. Oertel, J. Matschullat, K. Zurba, F. Zimmermann, S. Erasmi, Greenhouse gas emissions from soils—a review, Geochemistry 76 (3) (2016) 327–352, https://doi.org/10.1016/j.chemer.2016.04.002.
[3] S. Sen, D. Liu, G.T.R. Palmore, Electrochemical reduction of CO_2 at copper nanofoams, ACS Catal. 4 (9) (2014) 3091–3095, https://doi.org/10.1021/cs500522g.
[4] S. Lin, C.S. Diercks, Y.-B. Zhang, N. Kornienko, E.M. Nichols, Y. Zhao, A.R. Paris, D. Kim, P. Yang, O.M. Yaghi, C.J. Chang, Covalent organic frameworks comprising cobalt porphyrins for catalytic CO_2 reduction in water, Science 349 (6253) (2015) 1208–1213, https://doi.org/10.1126/science.aac8343.
[5] Y. Chen, S. Ji, C. Chen, Q. Peng, D. Wang, Y. Li, Single-atom catalysts: synthetic strategies and electrochemical applications, Joule 2 (7) (2018) 1242–1264, https://doi.org/10.1016/j.joule.2018.06.019.
[6] X.-Q. Li, G.-Y. Duan, X.-X. Yang, L.-J. Han, B.-H. Xu, Electroreduction of carbon dioxide to multi-electron reduction products using poly (ionic liquid)-based Cu-Pd catalyst, Fundam. Res. 2 (6) (2022) 937–945, https://doi.org/10.1016/j.fmre.2021.12.009.
[7] W. Choi, D.H. Won, Y.J. Hwang, Catalyst design strategies for stable electrochemical CO_2 reduction reaction, J. Mater. Chem. A. 8 (31) (2020) 15341–15357, https://doi.org/10.1039/D0TA02633F.
[8] L.D. Ramírez-Valencia, E. Bailón-García, F. Carrasco-Marín, A.F. Pérez-Cadenas, From CO_2 to value-added products: a review about carbon-based materials for electro-chemical CO_2 conversion, Catalysts 11 (3) (2021) 351, https://doi.org/10.3390/catal11030351.
[9] M. Li, E. Irtem, H.P. Iglesias van Montfort, M. Abdinejad, T. Burdyny, Energy comparison of sequential and integrated CO_2 capture and electrochemical conversion, Nat. Commun. 13 (2022) 5398, https://doi.org/10.1038/s41467-022-33145-8.
[10] B.H. Davis, Fischer-Tropsch synthesis: current mechanism and futuristic needs, Fuel Process. Technol. 1–3 (71) (2001) 157–166.
[11] H. Schulz, Short history and present trends of fischer–tropsch synthesis, Appl. Catal. Gen. 186 (1–2) (1999) 3–12, https://doi.org/10.1016/S0926-860X(99)00160-X.
[12] S.A. Mahyoub, F.A. Qaraah, C. Chen, F. Zhang, S. Yan, Z. Cheng, An overview on the recent developments of Ag-based electrodes in the electrochemical reduction of CO_2 to CO, Sustain. Energy Fuels 4 (1) (2020) 50–67, https://doi.org/10.1039/C9SE00594C.
[13] A. Salehi-Khojin, H.-R.M. Jhong, B.A. Rosen, W. Zhu, S. Ma, P.J.A. Kenis, R. I. Masel, Nanoparticle silver catalysts that show enhanced activity for carbon dioxide electrolysis, J. Phys. Chem. C. 117 (4) (2013) 1627–1632, https://doi.org/10.1021/jp310509z.
[14] Q. Lu, J. Rosen, Y. Zhou, G.S. Hutchings, Y.C. Kimmel, J.G. Chen, F. Jiao, A selective and efficient electrocatalyst for carbon dioxide reduction, Nat. Commun. 5 (1) (2014) 3242, https://doi.org/10.1038/ncomms4242.
[15] Y.-C. Hsieh, S.D. Senanayake, Y. Zhang, W. Xu, D.E. Polyansky, Effect of chloride anions on the synthesis and enhanced catalytic activity of silver nanocoral electrodes for CO 2 electroreduction, ACS Catal. 5 (9) (2015) 5349–5356, https://doi.org/10.1021/acscatal.5b01235.
[16] E. Lam, J.H.T. Luong, Carbon materials as catalyst supports and catalysts in the transformation of biomass to fuels and chemicals, ACS Catal. 4 (10) (2014) 3393–3410, https://doi.org/10.1021/cs5008393.
[17] K. Zhao, X. Quan, Carbon-based materials for electrochemical reduction of CO_2 to C 2+ oxygenates: recent progress and remaining challenges, ACS Catal. 11 (4) (2021) 2076–2097, https://doi.org/10.1021/acscatal.0c04714.
[18] Nanocarbons for Energy Conversion: Supramolecular Approaches; Nakashima, N., Ed.; Nanostructure Science and Technology; Springer International Publishing: Cham, 2019.
[19] K.P. Kuhl, E.R. Cave, D.N. Abram, T.F. Jaramillo, New insights into the electrochemical reduction of carbon dioxide on metallic copper surfaces, Energy Environ. Sci. 5 (5) (2012) 7050, https://doi.org/10.1039/c2ee21234j.
[20] G. Díaz-Sainz, K. Fernández-Caso, T. Lagarteira, S. Delgado, M. Alvarez-Guerra, A. Mendes, A. Irabien, Coupling continuous CO_2 electroreduction to formate with efficient Ni-based anodes, J. Environ. Chem. Eng. 11 (2023), 109171, https://doi.org/10.1016/j.jece.2022.109171.
[21] C. Kim, H.S. Jeon, T. Eom, M.S. Jee, H. Kim, C.M. Friend, B.K. Min, Y.J. Hwang, Achieving selective and efficient electrocatalytic activity for CO_2 reduction using immobilized silver nanoparticles, J. Am. Chem. Soc. 137 (43) (2015) 13844–13850, https://doi.org/10.1021/jacs.5b06568.
[22] T. Fan, Q. Wu, Z. Yang, Y. Song, J. Zhang, P. Huang, Z. Chen, Y. Dong, W. Fang, X. Yi, Electrochemically driven formation of sponge-like porous silver nanocubes toward efficient CO_2 electroreduction to CO, ChemSusChem 13 (10) (2020) 2677–2683.
[23] S. Ma, R. Luo, J.I. Gold, A.Z. Yu, B. Kim, P.J.A. Kenis, Carbon nanotube containing Ag catalyst layers for efficient and selective reduction of carbon dioxide, J. Mater. Chem. A 4 (22) (2016) 8573–8578, https://doi.org/10.1039/C6TA00427J.
[24] C. Chen, X. Sun, X. Yan, Y. Wu, H. Liu, Q. Zhu, B.B.A. Bediako, B. Han, Boosting CO_2 electroreduction on N,P-Co-doped carbon aerogels, Angew. Chem. Int. Ed. 59 (27) (2020) 11123–11129, https://doi.org/10.1002/anie.202004226.
[25] C. Kim, K.M. Cho, K. Park, J.Y. Kim, G.-T. Yun, F.M. Toma, I. Gereige, H.-T. Jung, Cu/Cu_2O interconnected porous aerogel catalyst for highly productive electrosynthesis of ethanol from CO_2, Adv. Funct. Mater. 31 (32) (2021) 2102142, https://doi.org/10.1002/adfm.202102142.
[26] M. Abdinejad, M.K. Motlagh, M. Noroozifar, H.B. Kraatz, Electroreduction of carbon dioxide to formate using highly efficient bimetallic Sn–Pd aerogels, Mater. Adv. 3 (2) (2022) 1224–1230, https://doi.org/10.1039/D1MA01057C.
[27] J. Fricke, T. Tillotson, Aerogels: production, characterization, and applications, Thin Solid Films 297 (1–2) (1997) 212–223, https://doi.org/10.1016/S0040-6090(96)09441-2.
[28] R.P. Patel, N.S. Purohit, A.M. Suthar, An overview of silica aerogels, Int. J. ChemTech Res. 1 (4) (2009) 1052–1057.
[29] L. Keshavarz, M.R. Ghaani, J.D. MacElroy, N.J. English, A comprehensive review on the application of aerogels in CO_2-adsorption: Materials and characterisation, Chem. Eng. J. 412 (2021), 128604.
[30] M. Abdinejad, C. Ferrag, M.N. Hossain, M. Noroozifar, K. Kerman, H.B. Kraatz, Capture and electroreduction of CO_2 using highly efficient bimetallic Pd–Ag aerogels paired with carbon nanotubes, J. Mater. Chem. A 9 (21) (2021) 12870–12877, https://doi.org/10.1039/D1TA01834E.
[31] L.E. Nita, A. Ghilan, A.G. Rusu, I. Neamtu, A.P. Chiriac, New trends in bio-based aerogels, Pharmaceutics 12 (5) (2020) 449, https://doi.org/10.3390/pharmaceutics12050449.
[32] A. Verma, S. Thakur, G. Goel, J. Raj, V.K. Gupta, D. Roberts, V.K. Thakur, Bio-based sustainable aerogels: new sensation in CO_2 capture, Curr. Res. Green. Sustain. Chem. 3 (2020), 100027, https://doi.org/10.1016/j.crgsc.2020.100027.
[33] S. Gong, X. Xiao, W. Wang, D.K. Sam, R. Lu, Y. Xu, J. Liu, C. Wu, X. Lv, Silk fibroin-derived carbon aerogels embedded with copper nanoparticles for efficient electrocatalytic CO_2-to-CO conversion, J. Colloid Interface Sci. 600 (2021) 412–420, https://doi.org/10.1016/j.jcis.2021.05.054.
[34] N. Falcone, T. Shao, N.M.O. Andoy, R. Rashid, R.M.A. Sullan, X. Sun, H.-B. Kraatz, Multi-component peptide hydrogels – a systematic study incorporating biomolecules for the exploration of diverse, tuneable biomaterials, Biomater. Sci. 8 (20) (2020) 5601–5614, https://doi.org/10.1039/D0BM01104E.
[35] M.A. Greenfield, J.R. Hoffman, M. Olvera de la Cruz, S.I. Stupp, Tunable mechanics of peptide nanofiber gels, Langmuir 26 (5) (2010) 3641–3647, https://doi.org/10.1021/la9030969.
[36] J. Raeburn, A. Zamith Cardoso, D.J. Adams, The importance of the self-assembly process to control mechanical properties of low molecular weight hydrogels, Chem. Soc. Rev. 42 (12) (2013) 5143, https://doi.org/10.1039/c3cs60030k.
[37] L. Wang, J. Lin, Phenylalanine-rich peptide mediated binding with graphene oxide and bioinspired synthesis of silver nanoparticles for electrochemical sensing, Appl. Sci. 7 (2) (2017) 160, https://doi.org/10.3390/app7020160.
[38] T. Kuila, S. Bose, C.E. Hong, M.E. Uddin, P. Khanra, N.H. Kim, J.H. Lee, Preparation of functionalized graphene/linear low density polyethylene composites by a solution mixing method, Carbon 49 (3) (2011) 1033–1037, https://doi.org/10.1016/j.carbon.2010.10.031.
[39] S. Zhao, S. Li, T. Guo, S. Zhang, J. Wang, Y. Wu, Y. Chen, Advances in Sn-based catalysts for electrochemical CO_2 reduction, Nano-Micro Lett. 11 (1) (2019) 62.
[40] Z. Sun, T. Ma, H. Tao, Q. Fan, B. Han, Fundamentals and challenges of electrochemical CO_2 reduction using two-dimensional, Mater. *Chem.* 3 (4) (2017) 560–587.
[41] K. Qi, Y. Zhang, J. Li, C. Charmette, M. Ramonda, X. Cui, Y. Wang, Y. Zhang, H. Wu, W. Wang, X. Zhang, D. Voiry, Enhancing the CO_2 -to-CO conversion from 2D silver nanoprisms via superstructure assembly, ACS Nano 15 (4) (2021) 7682–7693.
[42] T. Fan, Q. Wu, Z. Yang, Y. Song, J. Zhang, P. Huang, Z. Chen, Y. Dong, W. Fang, X. Yi, Electrochemically driven formation of sponge-like porous silver nanocubes toward efficient CO_2 electroreduction to CO, Chem. Sus. Chem. 13 (10) (2020) 2677–2683.
[43] W. Wang, S. Gong, J. Liu, Y. Ge, J. Wang, X. Lv, Ag-Cu Aerogel for Electrochemical CO_2 Conversion to CO, J. Colloid Interface Sci. 595 (2021) 159–167.
[44] K. Jiang, P. Kharel, Y. Peng, M.K. Gangishetty, H.-Y.G. Lin, E. Stavitski, K. Attenkofer, H. Wang, Silver nanoparticles with surface-bonded oxygen for highly selective CO_2 reduction, ACS Sustain. Chem. Eng. 5 (2017) 8529–8534.
[45] F. Mattarozzi, N. Visser, J.W. de Rijk, P. Ngene, P. de Jongh, Ligand-free silver nanoparticles for CO_2 electrocatalytic reduction to CO, Eur. J. Inorg. Chem. 29 (2022), e202200365.

[46] S. Li, X. Dong, W. Chen, Y. Song, G. Li, W. Wei, Y. Sun, Efficient CO_2 electroreduction over silver hollow fiber electrode, Catalysts 12 (453) (2022) 2–12.
[47] M.-J. Cheng, E.L. Clark, H.H. Pham, A.T. Bell, M. Head-Gordon, Quantum mechanical screening of single-atom bimetallic alloys for the selective reduction of CO_2 to C1 hydrocarbons, ACS Catal. 6 (2016) 7769–7777.
[48] Y. Pei, H. Zhong, F. Jin, A brief review of electrocatalytic reduction of CO_2-materials, reaction conditions, and devices, Energy Sci. Eng. 9 (2021) 1012–1032.
[49] Y. Hori, H. Wakebe, T. Tsukamoto, O. Koga, Electrocatalytic process of CO selectivity in electrochemical reduction of CO_2 at metal electrodes in aqueous media, Electro Acta 39 (1994) 1833–1839.
[50] N. Hoshi, M. Kato, Y. Hori, Electrochemical reduction of CO_2 on single crystal electrodes of silver Ag (111), Ag (100) and Ag (110), J. Electro Chem. 440 (1997) 283–286.
[51] X. Peng, S.G. Karakalos, W.E. Mustain, Preferentially oriented Ag nanocrystals with extremely high activity and faradaic efficiency for CO_2 electrochemical reduction to CO, ACS Appl. Mater. Interfaces 10 (2018) 1734–1742.
[52] H.A. Hansen, J.B. Varley, A.A. Peterson, J.K. Nørskov, Understanding trends in the electrocatalytic activity of metals and enzymes for CO_2 reduction to CO, J. Phys. Chem. Lett. 4 (2013) 388–392.
[53] M.J. Cheng, Y. Kwon, M. Head-Gordon, A.T. Bell, Theoretical investigations of the electrochemical reduction of CO on single metal atoms embedded in graphene, J. Phys. Chem. C. 119 (2015) 21345–21352.
[54] M. Karamad, V. Tripkovic, J. Rossmeisl, Intermetallic alloys as CO electroreduction catalysts-role of isolated active sites, J. ACS Catal. 4 (2014) 2268–2273.
[55] V. Tripkovic, M. Vanin, M. Karamad, M.E. Björketun, K.W. Jacobsen, K. S. Thygesen, J. Rossmeisl, Electrochemical CO_2 and CO reduction on metal-functionalized porphyrin-like graphene, J. Phys. Chem. C. 117 (2013) 9187–9195.
[56] B. Xiong, Y. Yang, J. Liu, Z. Hua, Y. Yang, Electrocatalytic reduction of CO_2 to C1 products over bimetal catalysts: a DFT screening study, Fuel Process. Technol. 233 (2022), 107315.